BMC Medical Imaging

RESEARCH

Open Access

Identification of SMAD4-mutated pancreatic ductal adenocarcinoma using preoperative contrast-enhanced MRI and clinical characteristics

Zhina Li[1,2†], Cheng Wang[1†], Jianbo Li[1†], Xingxing Wang[3], Xiang Li[3], Tianzhu Yu[4*], Jianjun Zhou[5], Xiaolin Wang[4], Mengsu Zeng[1] and Haitao Sun[1*]

Abstract

Aim To assess the value of preoperatively contrast-enhanced MRI and clinical characteristics for identification of SMAD4-mutated pancreatic ductal adenocarcinoma (PDAC) patients.

Materials and methods This retrospective study included patients with surgically confirmed PDAC from January 2016 to December 2022. Based on immunostaining results indicating the mutation of SMAD4, the enrolled participants were grouped into SMAD4-mutated PDAC and non-SMAD4-mutated PDAC. Contrast-enhanced MRI findings, clinical-pathological characteristics, and prognosis were recorded and reviewed. The pathological findings and clinical prognosis were compared between the two groups. Uni- and multivariable logistic regression analyses were further performed to determine the radiological and clinical predictive factors for the mutation of SMAD4.

Results In total, 428 PDAC patients were enrolled and analyzed, who were grouped as SMAD4-mutated PDAC ($n=224$) and non-SMAD4-mutated PDAC ($n=204$). SMAD4-mutated PDAC demonstrated higher frequency of pathological fatty infiltration (83.4% vs. 74.2%, $P=0.016$), peripheral nerve infiltration (84.4% vs. 76.5%, $P=0.039$). and higher recurrence rates (43.6% vs. 58.9%, $P=0.045$) than non-SMAD4-mutated PDAC. The 3-year recurrence-free survival rates were worse for SMAD4-mutated PDAC (28.7% vs. 39.1%). In multivariable logistic regression analyses, CA19-9 > 100 U/mL (odds ratio [OR] = 1.519, $P=0.041$), CBD dilation (OR = 1.564, $P=0.036$), and rim enhancement (OR = 1.631, $P=0.025$) were independent predictive factors.

†Zhina Li, Cheng Wang and Jianbo Li contributed equally to this work.

Haitao Sun and Tianzhu Yu contributed the same as corresponding authors.

*Correspondence:
Tianzhu Yu
yu.tianzhu@zs-hospital.sh.cn
Haitao Sun
sht1720@163.com

Full list of author information is available at the end of the article

Conclusion Rim enhancement, CBD dilation on contrast-enhanced MRI and higher CA19-9 level are promising radiological and clinical factors for identifying SMAD4-mutated PDAC.

Keywords Pancreatic ductal adenocarcinoma, Magnetic resonance imaging, Mutationp, Prognosis

Introduction

The incidence of pancreatic ductal adenocarcinoma (PDAC) has growingly risen in recent years [1]. Most pancreatic cancer PDAC originates from the ductal epithelium, and the overall 5-year survival rate is no higher than 10% [2]. Pancreatic cancer tissue exhibits high heterogeneity and complex gene mutations. These genetic variants are intimately closed to the biological behavior of PDAC, based on which the degree of malignancy, molecular subtypes, efficacy, and prognosis of PDAC can be stratified and predicted [3, 4].

SMAD4 (located on chromosome 18q21), known as *deleted in pancreatic carcinoma 4 (DPC4)*, is the most frequent mutated suppressor gene, which is a critical factor in the suppression of the tumorigenic activity of pro-inflammatory cytokines and the induction of arrest and apoptosis of precancerous cells [5]. *SMAD4*, occurred either by homozygous deletion or by intragenic mutations and loss of heterozygosity, is functioned as a key cofactor for improving gene transcription and tumor suppression via *the transforming growth factor-β (TGF-β)* signaling pathway [6]. Multiple studies indicated SMAD4-mutated PDAC shows a poorly biological behavior, such as poorly immunogenic molecular subtype (limited T-cell infiltration or PD-L1 expression) and adverse mechanophenotype or proliferation phenotypes [7–9]. M Tascilar and coworkers have reported PDAC patients with SMAD4 expression showed significantly longer survival than those loss of SMAD4 expression in (median survival was 19.2 months vs. 14.7 months) [8]. Various clinical studies have similarly observed PDAC patients lack SMAD4 expression is often associated with increased tumor progression, metastasis rate, and reduced overall survival [10, 11]. Notably, the dysregulation of SMAD4 is closely linked to chemotherapy resistance and the efficacy of radiotherapy in pancreatic ductal adenocarcinoma (PDAC), significantly influencing the development of clinical treatment strategies [12, 13].

In clinical practice, tumoral genetic status is commonly assessed using tumor specimens acquired from biopsy or surgery [14]. In addition, some new techniques, such as liquid biopsy, have gradually become alternative methods for identifying genetic status. Nevertheless, these commonly used clinical methods have the drawback of intrusiveness, expensiveness, and limited detectability, while the results obtained from samples from local tumor resection or biopsy may be unrepresentative due to the highly inherent heterogeneous of PDAC. Noninvasive imaging has also been applied to help predict genetic information of various tumors.

Non-invasive imaging techniques have been applied to assess pathological subtypes and the gene expression status of various tumors or diseases, and such imaging signature markers related to the disease genes expression and molecules have been screened for assessing curative efficacy and prognosis [15–17]. Notably, several imaging features have been shown to indicate different PDAC subtypes (e.g. adenosquamous carcinoma, mucinous carcinoma, and large duct carcinoma), which are associated with SMAD4 expression [18–20]. Moreover, several radiomics features have been filtered and shown to correlate with the mutational status of pancreatic cancer [21, 22]. For example, Ricarda Hinzpeter and coworkers have demonstrated CT-based radiomics features are correlated with TP53 and KRAS gene mutation in PDAC (Youden index = 0.67 and 0.56) [22]. Unfortunately, studies of such noninvasive imaging to assess PDAC are still rare and in the preliminary stages.

Despite the prevalence of SMAD4-mutated PDAC, its imaging characteristics are not still unclear. Hence, our study proposed to determine whether contrast-enhanced MRI imaging can differentiate the status of SMAD4 in pancreatic cancer and to identify the clinical and imaging predictive factors for SMAD4 mutation in PDAC.

Materials and methods

Study design and patients

This study has been approved by the Institutional Review Committee of Zhongshan Hospital, Fudan university (approval no. B2024-250R). Owing to its retrospective nature, the need for obtaining written informed consent was exempted. Clinical trial number: not applicable.

This retrospective study included 1216 patients diagnosed with operatively pathologically confirmed pancreatic ductal adenocarcinoma (PDAC) from Zhongshan hospital, Fudan University between January 2016 to December 2022. All consecutive patients with surgically pathology-confirmed PDAC were reviewed and screened. Ultimately, a total of 428 eligible PDAC patients were enrolled, who also met the following inclusion criteria (Fig. 1): (I) histologically and surgically confirmed PDAC; (II) availability of comprehensive pathological analysis, including immunohistochemical evaluation of expression of SMAD4; (III) preoperative MRI performed with gadolinium-based contrast, multiphasic acquisition, T2-weighted, and diffusion-weighted imaging (DWI) sequences; (IV) available follow-up imaging, comprising

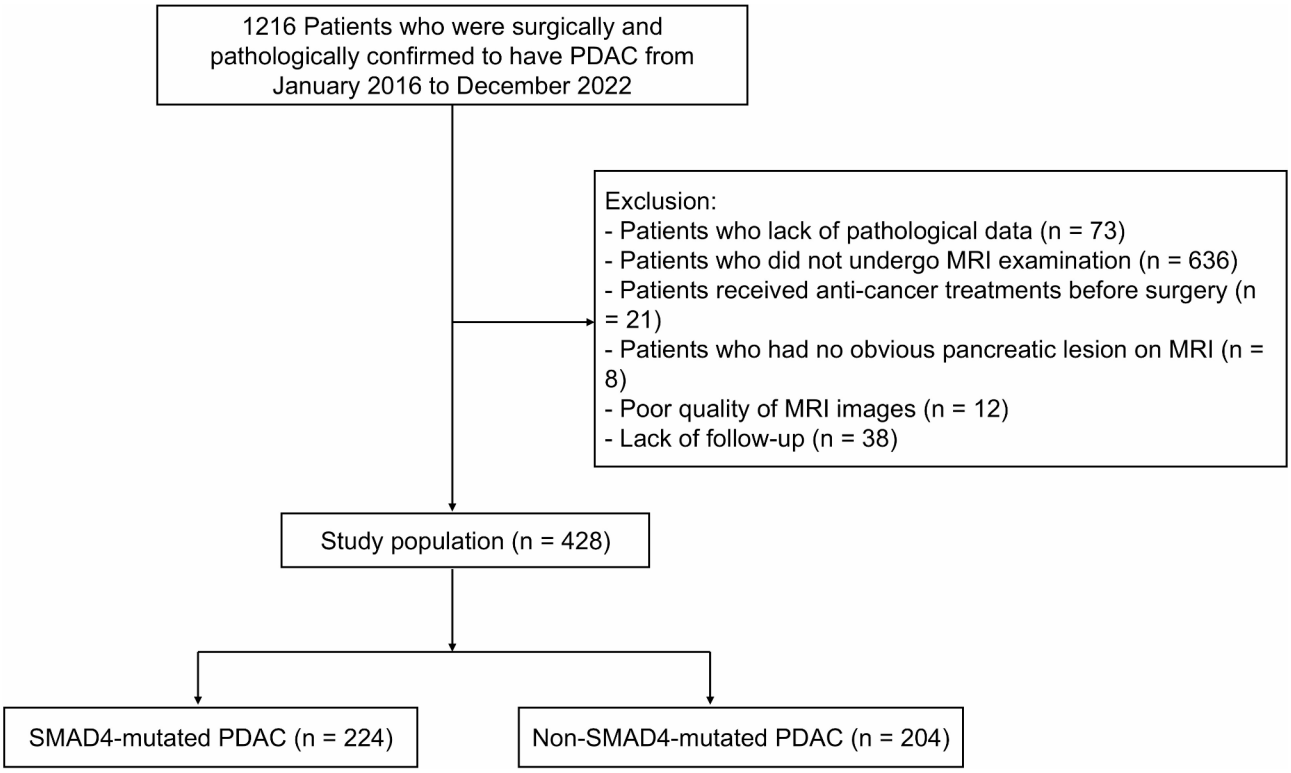

Fig. 1 The enrolled patient flowchart

CT and/or MRI, conducted at predefined intervals (every 3 to 6 months).

Clinical, laboratory and pathological data analysis

Clinical and laboratory data including such as age, sex, body mass index (BMI), diabetes, high blood pressure (HBP), smoking history, drinking history, resection margin (R0/R1), T and N stages according to the eighth edition of the American Joint Committee on Cancer (AJCC) staging system, and laboratory markers of total bilirubin (TBil), albumin, and serum tumor markers of CA199 and were collected. Pathological data including histologic grade, vascular invasion, peripheral nerve infiltration, and Ki-67 expression status were recorded.

The prognosis data including recurrence-free survival (RFS) and overall survival (OS) were recorded and analyzed. Recurrence was characterized as evidence of disease on postoperative radiological images, and RFS was calculated between the data of surgery and the data of recurrence, last clinical follow-up, or death. The OS was calculated from the surgical date until death for any reason or until the last follow-up. The average follow-up period was 697.6 (median, 497 days; interquartile range, 263.8–921.3 days) and 513.9 (median, 324.5 days; interquartile range, 172.8–649.0 days) days for OS and RFS.

Histologic diagnosis and immunohistochemistry

Immunohistochemistry of SMAD4 was conducted for all enrolled samples and classified into SMAD4-mutated PDAC and non-SMAD4-mutated PDAC. The diagnostic process for immunohistochemical staining analysis is as follows: The expression of SMAD4 in the sample was detected using the automated immunohistology-chemical detection system (Leica Bond max Sys). The slides were labeled with monoclonal antibodies to SMAD4 (B8, Santa Cruz Biotechnology, Dallas, TX), and the presence of brown staining in the nuclei of tumor cells was defined as a positive reaction. The known immunohistochemical positive control tissues were selected as positive controls, and PBS was used as a negative control instead of antibody. Two pathologists (X.L. and X.X.W with 6 and 14 years of experience, respectively), who were unaware of sequencing results and clinical outcomes, assessed the immunohistochemistry staining of the tumor specimens, and the unified opinions of the two pathologists were used for subsequent analysis.

Imaging analyses

All patients performed contrast-enhanced MRI at 1.5 T (MAGNETOM Aera, Siemens) and 3.0 T (Prisma, Siemens) (Table S1-2). During dynamic-enhanced phases, the arterial phase data was captured once the contrast agent (gadolinium diethylenetriamine pentaacetic acid, Gd-DTPA; Magnevist, Bayer HealthCare) entered the

ascending aorta, following intravenous injection at a dose of 0.1 mmol/kg and a rate of 2 mL/s. Subsequently, the portal venous phase and delayed phase sequences were obtained at 70–90 s and 160–180 s, respectively.

The MR images were reviewed on a PACS workstation by tree radiologists (Z.N.L, J.J.Z, M.S.Z. with 10, 28, and 35 years of abdominal imaging experience, respectively) blinded to the clinical data. The consensus of the three radiologists was used for subsequent analysis.

For the morphological MRI characteristics, the tumor location (head/body or tail) tumor size, margin (well-/ill-defined), and location (head/neck, body or tail) were measured by the two observers. The signal intensity on T2-weighted, diffusion-weighted images (DWI), unenhanced T1-weighted, arterial (API), portal venous (VPI), and delayed phase images (DPI) were classified as hypointense or iso-/hyper-intense compared with the surrounding pancreatic parenchyma. Accompanying findings, including tumor texture, common bile duct (CBD) dilation, main pancreatic duct (MPD) dilation, intrahepatic bile duct (IBD) dilation, pancreatic atrophy, peripancreatic fat infiltration, cystic degeneration, hemorrhage, necrotic, enlarged lymph nodes at imaging, and rim enhancement were evaluated [23, 24]. The MPD, CBD, and IBD were respectively considered to have dilation if their diameters were 3 mm, 10 mm, or 3 mm or greater [25]. Rim enhancement was described as the presence of a ring-shaped intensification encircling a comparatively hypo-intensity central region [26]. A comprehensive explanation of the rest imaging characteristics mentioned above is provided in Appendix S1. For quantitative assessment, the apparent diffusion coefficient (ADC) value of the tumor was determined through DWI. Regions of interest were positioned at the tumor's widest point, and the borders of the lesion were manually traced to encompass the broadest tumor expanse. The average of measurements by three radiologists was used for analysis.

Table 1 Patient clinical characteristics

Characteristics	Non-SMAD4-mutated PDAC (*n* = 204)	SMAD4-mutated PDAC (*n* = 224)	*P* value
Age	64.74 ± 9.27	64.57 ± 9.03	0.850
Sex			
Male	115(56.37%)	131(58.48%)	0.659
Female	89(43.63%)	93(41.52%)	
BMI	22.69 ± 3.16	22.82 ± 3.26	0.708
Diabetes			0.247
Absence	148(72.55%)	151(67.41%)	
Presence	56(27.45%)	73(32.59%)	
HBP			0.647
Absence	113(55.39%)	129(57.59%)	
Presence	91(44.61%)	95(42.41%)	
CA19-9 (U/mL)			**0.010**
> 100	94(46.08%)	76(33.93%)	
≤ 100	110(53.92%)	148(66.07%)	
TBil (μmol/L)			0.245
> 20.4	65(31.86%)	83(37.05%)	
≤ 20.4	139(68.14%)	140(62.5%)	
Albumin (g/L)			0.373
> 37	169(82.84%)	178(79.46%)	
≤ 37	35(17.16%)	46(20.54%)	
T stage			0.427
T1	62(30.39%)	58(25.89%)	
T2	109(53.43%)	136(60.71%)	
T3	32(15.69%)	28(12.5%)	
T4	4 (0.49%)	1 (0.9%)	
N stage			0.527
N0	120(58.82%)	122(54.46%)	
N1	73(35.78%)	85(37.95%)	
N2	11(5.39%)	17(7.59%)	
Resection margin			0.180
R0	199(97.55%)	213(95.09%)	
R1	5(2.45%)	11(4.91%)	

PDAC = pancreatic ductal adenocarcinoma, BMI = body mass index, HBP = high blood pressure; TBil = total bilirubin, CA 19 − 9 = cancer antigen 19 − 9

Statistical analysis

The clinical, pathological, and radiological comparisons between two groups were analyzed using Mann-Whitney and χ^2 tests. For clinical-radiological characteristics with statistically significant differences in univariate analyses, multi-variable regression analyses were further performed to screen significant independent predictors. The Kaplan-Meier analyses, employing the log-rank test, were utilized to compare the survival curves (OS and RFS) between the two groups. The interobserver agreement was conducted via the κ coefficient. The kappa value was defined as follows: 0.00–0.20, poor; 0.21–0.40, fair; 0.41–0.60, moderate; 0.61–0.80, well; and 0.81–1.00, excellent [27]. All statistical analyses were performed using SPSS 26 software, IBM, Armonk, NY and R software (version 4.3.2). A P-value of less than 0.05 was considered statistically significant.

Results

Patient characteristics

In the present study, a total of 1216 PDAC patients were retrospectively reviewed. 788 patients were excluded from the analysis due to not meeting the inclusion criteria for this study (Fig. 1). Finally, 428 PDAC patients (median age, 64.66 ± 9.15 years) were enrolled in our study with a male to female ratio of 1.35:1. In our cohort, the enrolled patients were divided into non-SMAD4-mutated (204, 47.6%) and SMAD4-mutated PDAC groups. There were no significant differences in several clinical features, such as age, sex, BMI, HBP, and diabetes (P = 0.274–0.708; Table 1). Sixteen patients (3.7%) had positive surgical margins (R1), and there was no statistically significant difference between the SMAD4-mutated and non-SMAD4-mutated groups.

Moreover, SMAD4-mutated PDAC showed higher serum CA19-9 levels compared to non-SMAD4-mutated PDAC (median, 157.8 U/mL vs. 115.5 U/mL; $P=0.010$). However, there was no obvious difference in serum TBiL and albumin levels between the two groups. At multivariable analysis, CA19-9 was a predictive factor of P53-mutated PDAC (odds ratio, 1.519; 95% CI: 1.017, 2.268; $P=0.041$). Table 1 shows the detailed clinical characteristics of enrolled patients.

Imaging characteristics for identifying SMAD4-mutated PDAC

In our cohort, SMAD4-mutated PDAC showed more frequent ill-defined margin (99 of 224 [44.2%] vs. 70 of 204 [34.3%]; $P=0.037$), CBD dilation (91 of 224 [40.6%] vs. 62 of 204 [30.4%]; $P=0.027$) and necrotic region (99 of 224 [44.2%] vs. 62 of 204 [30.4%]; $P=0.035$), rim enhancement (133 of 224 [59.4%] vs. 91 of 204 [44.6%]; $P=0.002$) in contrast-enhanced MRI (Table 2).

Table 2 Patient radiological characteristics

Characteristics	Non-SMAD4-mutated PDAC ($n=204$)	SMAD4-mutated PDAC ($n=224$)	*P* value
Location			0.325
Head	118(57.84%)	140(62.5%)	
Body/tail	86(42.16%)	84(37.5%)	
Size	2.929 ± 1.118	2.942 ± 1.028	0.900
Margin			**0.037**
Well-defined	134(65.69%)	125(55.8%)	
Ill-defined	70(34.31%)	99(44.2%)	
Signal in T2-weighted images			0.445
Hypointense	51(25%)	49(21.88%)	
Iso-/hyper-intense	153(75%)	175(78.13%)	
Signal in DWI			0.617
Iso-/hyper-intense	45(22.06%)	45(20.09%)	
Hyperintense	159(77.94%)	179(79.91%)	
Unenhanced T1-weighted imaging			0.635
Hypointense	184(90.2%)	205(91.52%)	
Iso-/hyper-intense	20(9.8%)	19(8.48%)	
API at MRI			0.622
Hypointense	177(86.76%)	197(87.95%)	
Iso-/hyper-intense	27(13.24%)	26(11.61%)	
VPI at MRI			0.787
Hypointense	137(67.16%)	147(65.63%)	
Iso-/hyper-intense	67(32.84%)	76(33.93%)	
DPI at MRI			0.513
Hypointense	96(47.06%)	112(50%)	
Iso-/hyper-intense	108(52.94%)	111(49.55%)	
MPD dilation			0.224
Absence	73(35.78%)	93(41.52%)	
Presence	131(64.22%)	131(58.48%)	
CBD dilation			**0.027**
Absence	142(69.61%)	133(59.38%)	
Presence	62(30.39%)	91(40.63%)	
IBD dilation			0.349
Absence	139(68.14%)	143(63.84%)	
Presence	65(31.86%)	81(36.16%)	
Peripancreatic fat infiltration			0.983
Absence	39(19.12%)	43(19.2%)	
Presence	165(80.88%)	181(80.8%)	
Pancreatic atrophy			0.653
Absence	114(55.88%)	130(58.04%)	
Presence	90(44.12%)	94(41.96%)	
Cystic degeneration			0.638
Absence	163(79.9%)	183(81.7%)	
Presence	41(20.1%)	41(18.3%)	

Table 2 (continued)

Characteristics	Non-SMAD4-mutated PDAC (*n* = 204)	SMAD4-mutated PDAC (*n* = 224)	*P* value
Hemorrhage			0.384
Absence	201(98.53%)	218(97.32%)	
Presence	3(1.47%)	6(2.68%)	
Necrotic			**0.035**
Absence	142(69.61%)	134(59.82%)	
Presence	62(30.39%)	90(40.18%)	
Enlarged lymph nodes at imaging			0.877
Absence	148(72.55%)	164(73.21%)	
Presence	56(27.45%)	60(26.79%)	
ADC ($\times 10^{-3}$ mm^2/s)	1.412 (1.204–1.661)	1.404 (1.206–0.634)	0.579
Rim enhancement			**0.002**
Absence	113(55.39%)	91(40.63%)	
Presence	91(44.61%)	133(59.38%)	

PDAC = pancreatic ductal adenocarcinoma, API = arterial phase intensity, VPI = venous phase intensity, DPI = delayed phase intensity, MPD = main pancreatic duct, CBD = common bile duct, IBD = Intrahepatic bile duct, ADC = apparent diffusion coefficient

Table 3 Uni- and multi-variate analyses for predictive factors for SMAD4 mutation of PDAC

Predictive factors	Univariate Analysis		Multivariate Analysis	
	OR (95% CI)	*P* value	OR (95% CI)	*P* value
Age	1.002 (0.981, 1.023)	0.849		
Sex [Male]	0.917 (0.625, 1.346)	0.659		
BMI	1.011 (0.953, 1.073)	0.707		
Diabetes[present]	1.278 (0.843, 1.936)	0.248		
HBP [present]	0.914 (0.624, 1.341)	0.647		
CA19-9 [> 100 U/mL]	1.631 (1.105, 2.409)	**0.014**	1.519 (1.017, 2.268)	**0.041**
TBil (μmol/L) [> 20.4 μmol/L]	1.268 (0.849, 1.892)	0.246		
Albumin [> 37 g/L]	1.248 (0.766, 2.032)	0.373		
Resection margin [R1]	2.055 (0.702, 6.020)	0.189		
Location [Head]	0.823 (0.559, 1.213)	0.326		
Size	1.011 (0.847, 1.208)	0.900		
Margin [Ill-defined]	1.516 (1.025, 2.242)	**0.037**	1.283 (0.845, 2.377)	0.242
Signal in T2-weighted images [Hyperintense]	1.126 (0.707, 1.783)	0.618		
Signal in DWI [Hyperintense]	1.190 (0.761, 1.863)	0.446		
Unenhanced T1-weighted imaging [Hypointense]	1.173 (0.607, 2.266)	0.635		
API at MRI [Hypointense]	1.156 (0.650, 2.055)	0.622		
VPI at MRI [Hypointense]	0.946 (0.632, 1.415)	0.787		
DPI at MRI [Hypointense]	1.135 (0.776, 1660)	0.513		
MPD dilation [present]	0.900 (0.588, 1.377)	0.628		
CBD dilation [present]	1.567 (1.050, 2.338)	**0.028**	1.564 (1.029, 2.268)	**0.036**
IBD dilation [present]	1.211 (0.811, 1.809)	0.349		
Peripancreatic fat infiltration [present]	0.995 (0.614, 1.611)	0.983		
Pancreatic atrophy [present]	0.916 (0.624, 1.344)	0.653		
Cystic degeneration [present]	0.891 (0.550, 1.442)	0.891		
Hemorrhage [present]	1.844 (0.455, 7.471)	0.391		
Necrotic [present]	1.538 (1.031, 2.296)	**0.035**	1.224 (0.773, 1.939)	0.388
Enlarged lymph nodes at imaging [present]	0.967 (0.631, 1.481)	0.877		
ADC ($\times 10^{-3}$ mm^2/s)	1.142 (0.714, 1.827)	0.578		
Rim enhancement [present]	1.815 (1.236, 2.664)	**0.002**	1.631 (1.064, 2.498)	**0.025**

PDAC = pancreatic ductal adenocarcinoma, OR = Odds ratio; CI = confidence interval; ADC = apparent diffusion coefficient; API = arterial phase intensity, VPI = venous phase intensity, DPI = delayed phase intensity, MPD = main pancreatic duct, CBD = common bile duct, IBD = Intrahepatic bile duct

The results of the univariate and multivariate analyses of the clinical and radiological characteristics for identifying SMAD4-mutated PDACs in present cohort are showed in Table 3. Of all, CA19-9 > 100 U/mL (odds ratio [OR] = 1.519, 95% CI: 1.017, 2.268, $P = 0.041$), the presence of CBD dilation (OR = 1.564, 95% CI: 1.029,

2.268, $P=0.036$), and the presence of rim enhancement (OR=1.631, 95% CI: 1.064, 2.498; $P=0.025$) were independent predictive factors of SMAD4-mutated PDAC (Figs. 2 and 3).

In terms of interobserver agreement for MRI features, the two observers exhibited well interobserver agreement for enlarged lymph nodes at imaging, Hemorrhage, and ADC (κ=0.735–0.786) and excellent agreement for remaining other variables (κ=0.809–0.976) (Table S3).

Pathological characteristics

In our cohort, SMAD4-mutated PDAC showed more frequent pathological fatty infiltration and peripheral nerve infiltration than non-SMAD4-mutated PDAC (187 of 224 [83.4%] vs. 151 of 204 [74.2%]; $P=0.016$; 189 of 224 [84.4%] vs. 156 of 204 [76.5%]; $P=0.039$) (Table 4). However, the histologic grade, pathological lymphovascular invasion, and Ki-67 expression status were no significant between SMAD4-mutated and non-SMAD4-mutated

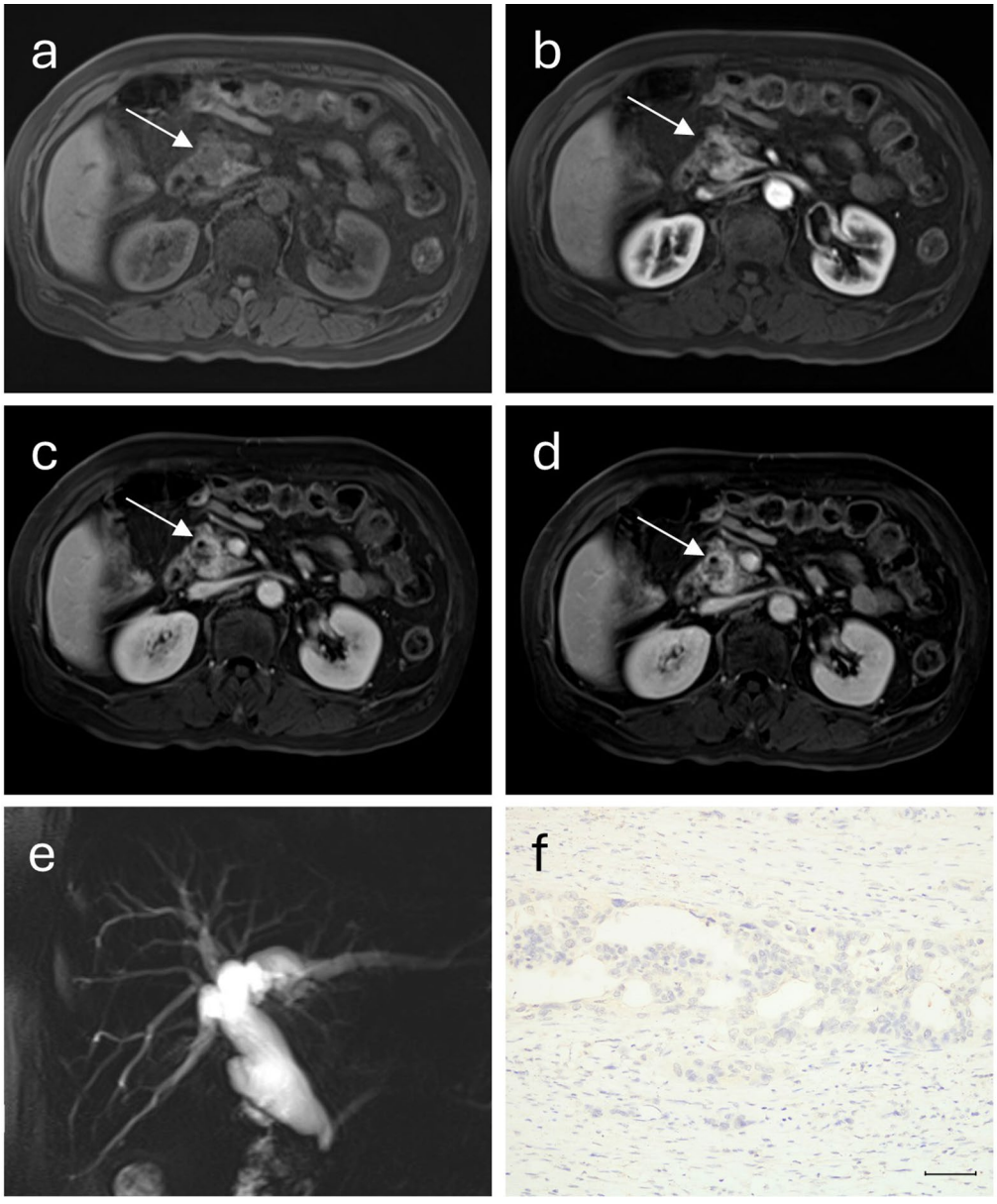

Fig. 2 Images depict non-SMAD4-mutated PDAC located in the head of the pancreas with a CA19-9 level of 1819.0 U/mL. The series includes unenhanced transverse images(**a**), contrast-enhanced images in the arterial phase (**b**), venous phase(**c**), and delayed phase (**d**) T1W images, illustrating a 2.2-cm mass without rim enhancement (arrows). (**e**) MRCP illustrates dilation of the common bile duct (CBD). (**f**) SMAD4 immunostaining reveals negative expression in the nuclei of the tumor cells (scale bar = 30 μm)

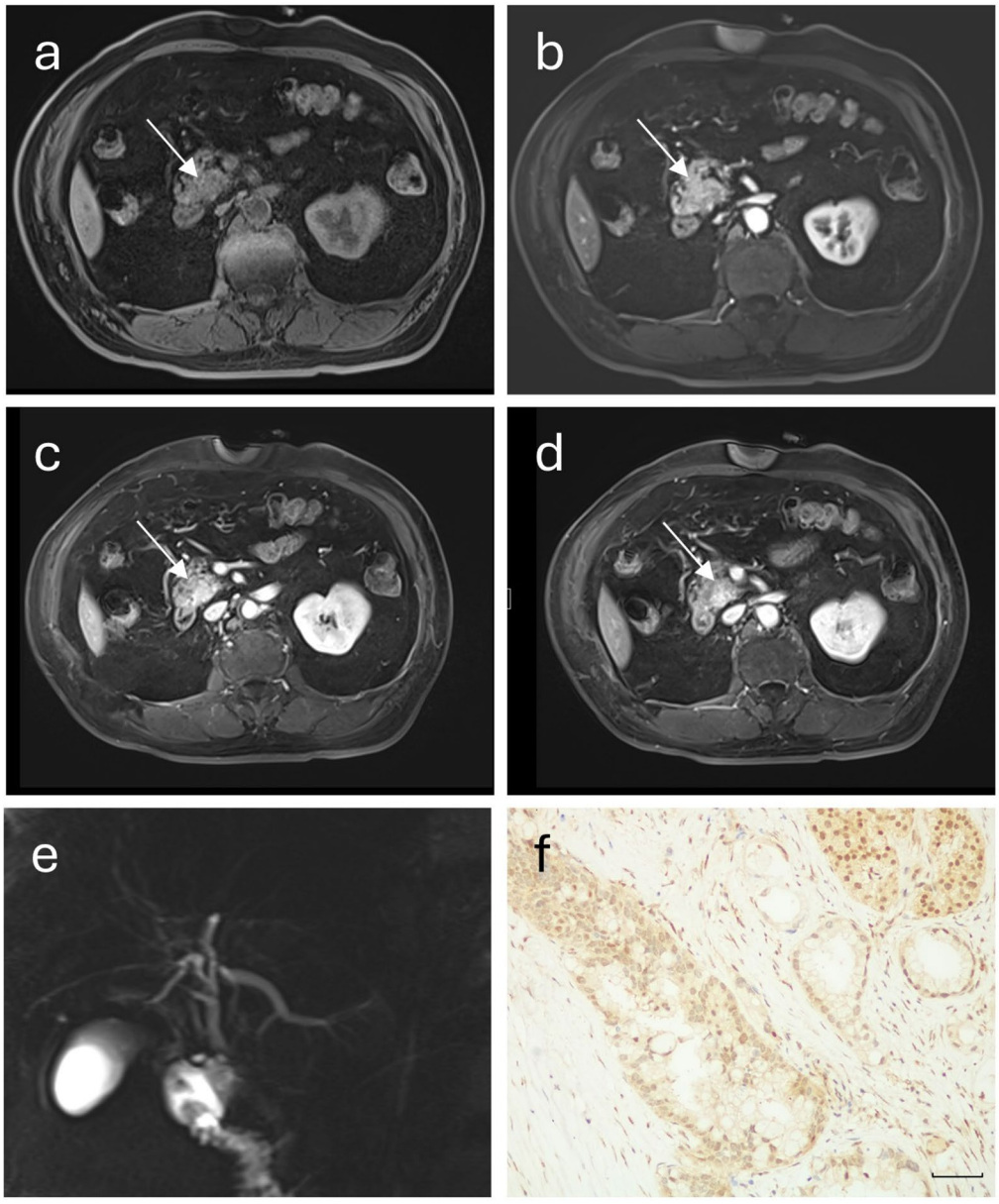

Fig. 3 The images depict a case of non-SMAD4-mutated PDAC located in the head of the pancreas with a CA19-9 level of 61.8 U/mL. The series includes unenhanced transverse images(**a**), contrast-enhanced images in the arterial phase (**b**), venous phase(**c**), and delayed phase (**d**) T1W images, illustrating a 3.3-cm low-signal-intensity mass without rim enhancement (arrows). (**e**) MRCP illustrates dilation-free of the CBD. (f) SMAD4 immunostaining reveals intense expression within the nuclei of the tumor cells (scale bar = 30 μm)

PDAC (P=0.249–0.951). In terms of interobserver agreement, the two pathologists exhibited excellent interobserver agreement for the SMAD4 expression (κ=0.939).

Prognosis

In our cohort, SMAD4-mutated PDAC showed higher recurrence rates than non-SMAD4-mutated PDAC (132 of 224 [43.6%] vs. 89 of 204 [58.9%]; P=0.045). However, the lymph node metastasis (102 of 224 [45.5%] vs. 84 of 204 [41.8%]; P=0.364) rate was no significant difference between SMAD4-mutated and non-SMAD4-mutated PDAC. In present cohort, the 1-, 3-, 5-year overall survival rate was 91.7%, 53.7%, and 44.8% for patients with non-SMAD4-mutated PDAC, whereas it was 86.4%, 50.7%, and 41.3% for patients with SMAD4-mutated PDAC, showing no discernible differences (P=0.34) (Fig. 4a). The 1-, 3-, and 5-year recurrence-free survival rates for patients with SMAD4-mutated PDAC were 58.6%, 28.7%, and 20.4%, significantly lower than the 65.0%, 40.6%, and 31.5% rates in patients non-SMAD4-mutated PDAC (P=0.045) (Fig. 4b).

Table 4 Analysis of pathologic features for the correlation with SMAD4 mutation of PDAC

Characteristics	Non-SMAD4-mutated PDAC (*n* = 204)	SMAD4-mutated PDAC (*n* = 224)	*P* value
Histologic grade			0.951
Well-differentiated	5(2.45%)	5(2.23%)	
Moderately differentiated	120(58.82%)	135(60.27%)	
Ill-differentiated	79(38.73%)	84(37.5%)	
Pathological fatty infiltration			**0.016**
Absence	53(25.98%)	37(16.52%)	
Presence	151(74.02%)	187(83.48%)	
Pathological peripheral nerve infiltration			**0.039**
Absence	48(23.53%)	35(15.63%)	
Presence	156(76.47%)	189(84.38%)	
Pathological lymphovascular invasion			0.249
Absence	154(75.49%)	158(70.54%)	
Presence	50(24.51%)	66(29.46%)	
Ki-67 expression status			0.490
≥ 50%	120(58.82%)	125(55.8%)	
< 50%	83(40.69%)	99(44.2%)	

PDAC = pancreatic ductal adenocarcinoma, BMI = body mass index, HBP = high blood pressure; TBil = total bilirubin, CA 19 − 9 = cancer antigen 19 − 9

Discussion

In this study, we evaluated the utility of contrast-enhanced MRI alongside clinical characteristics in identifying and assessing the SMAD4 mutation status in PDAC. Our study has demonstrated that SMAD4-mutated PDAC is associated with higher levels of CA19-9 > 100 U/mL (OR = 1.519, P = 0.041), CBD dilation (OR = 1.564, P = 0.036), and rim enhancement (OR = 1.631, P = 0.025) in multivariate analysis. Moreover, SMAD4-mutated PDAC is more frequently associated with pathological fatty infiltration (P = 0.016), peripheral nerve infiltration (P = 0.039), and a worse recurrence-free survival (P = 0.045) compared to non-SMAD4-mutated PDAC.

Previous research has highlighted the potential of imaging modalities to predict gene mutation status in PDAC. For instance, the rim enhancement on dynamic contrast-enhanced MRI is closely linked to PDAC with a high KRAS variant allele frequency [28]. In addition, radiomics based on CT and multiparametric magnetic resonance imaging showed promising capacity for differentiating various gene mutation of PDAC, such as TP53 and SMAD4 [21, 29]. However, the specific imaging features associated with different mutant phenotypes of pancreatic cancer remain inadequately characterized. Given that SMAD4 is one of the most frequently inactivated tumor suppressor genes in PDAC, understanding its relationship with imaging features is crucial. Our study, which found SMAD4 mutations in 52.3% of patients, consistent with prior reports, is among the first to specifically delineate MRI features associated with SMAD4-mutated PDAC, providing a distinct clinical-imaging risk profile [30, 31].

Our study verified a greater occurrence of rim enhancement on contrast-enhanced MRI among patients with SMAD4-mutated PDAC. It has been reported that rim enhancement feature is associated with poor prognosis in PDAC. A retrospective study showed that rim enhancement on at dynamic-enhanced MR imaging is a preoperative prognostic factor that affect disease-free survival (DFS) and OS after curative resection of PDAC [26]. Moreover, rim enhancement on MDCT has been identified as a risk factor for occult metastasis [23]. This feature likely reflects the necrotic core and surrounding viable tumor cells, which is indicative of more aggressive tumor biology. The association between higher KRAS mutation frequencies and rim-enhancing PDAC further supports this relationship. Our findings suggest that the poorer RFS seen in SMAD4-mutated PDAC could be partly due to the propensity of these tumors to exhibit rim enhancement on MRI, reflecting their more aggressive nature.

CBD dilation is more frequently observed in SMAD4-mutated PDAC in our cohort. The CBD and MPD dilation, commonly co-referred as the "double duct sign" is considered as a well-recognized malignant indicator of PDAC [32, 33]. The signs of bile duct dilation like this are not only related to the location of the tumor but also, to some extent, associated with the infiltrative nature, gene phenotype, and prognosis of the pancreatic tumor [34]. For example, the *GNAS* mutation was significantly associated with MPD dilation in intraductal papillary mucinous neoplasms [35]. Moreover, CBD or MPD dilation are independent risk factors for pancreatic neuroendocrine tumor with poor DFS [36]. In our cohort, the proportion of MPD dilation was higher than that of CBD, but there was no statistical difference between the SMAD4-mutated and non- SMAD4-mutated groups. However, the dilation of the CBD was more likely to occur in the SMAD4-mutated PDAC group. This may be due to the higher cellular infiltrative capacity of SMAD4-mutated PDAC, which leads to a more extensive degree and range of invasion.

In addition to radiological features, elevated preoperative serum CA19-9 levels (>100 U/mL) were associated with SMAD4 mutation. CA19-9, a widely used biomarker in PDAC, has been linked to tumor burden, treatment response, and genetic phenotype [37–39]. For instance, higher CA19-9 levels have been correlated with KRAS-mutated circulating tumor DNA in PDAC [40]. In our cohort, SMAD4-mutated PDAC exhibits a higher recurrence rate. This poor prognostic biological behavior may explain its correlation with higher levels of CA19-9. However, in this study, other clinical characteristics do

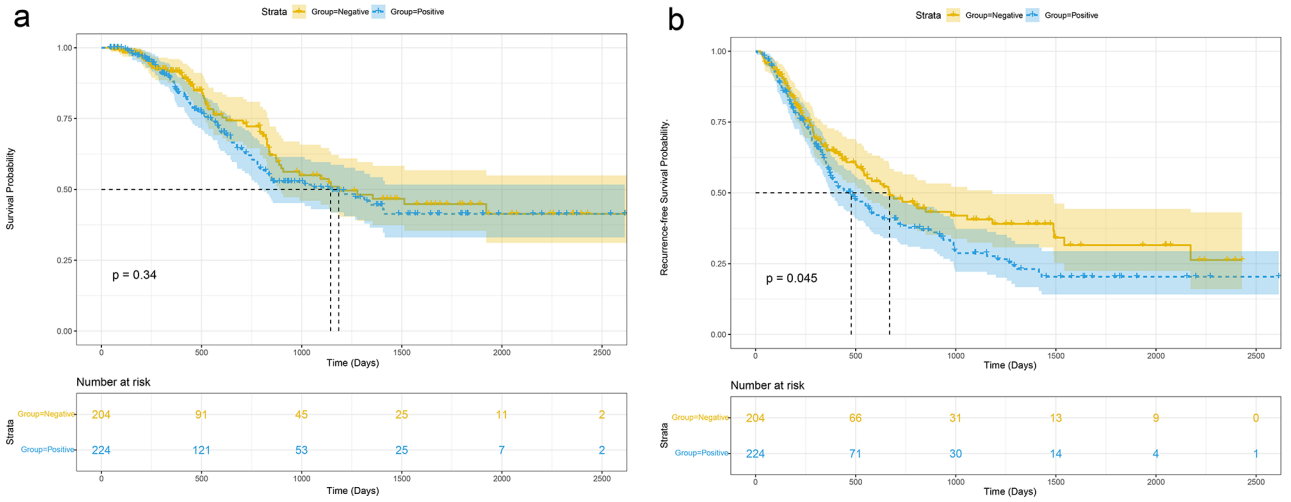

Fig. 4 Kaplan-Meier curves illustrate (**a**) overall survival and (**b**) recurrence-free survival rates in patients with SMAD4-mutated and non-SMAD4-mutated PDAC. The overall survival rate among patients with SMAD4-mutated PDAC did not significantly differ from those with non-SMAD4-mutated PDAC ($P=0.32$). However, patients with SMAD4-mutated PDAC exhibited significantly lower recurrence-free survival rates compared to those with non-SMAD4-mutated PDAC ($P=0.045$). Positive and negative groups represent SMAD4-mutated and non-SMAD4-mutated PDAC, respectively

not have discriminatory significance for SMAD4 mutation in PDAC. Notably, the sensitivity of CA19-9 varies depending on the clinical context, particularly in patients with cholestasis or biliary obstruction, where elevated bilirubin levels can impact CA19-9 levels. Although CA19-9 holds promise as a biomarker for SMAD4 mutation, its specificity is limited. Combining CA19-9 with imaging features may enhance predictive accuracy.

There are several limitations to our study. Firstly, this is a single-center retrospective study and addressing its inherent selection bias presents a notable challenge. Therefore, further multi-center, large-sample cohort studies are warranted in the future. Secondly, this study exclusively encompassed PDAC patients confirmed by surgical pathology, rendering our conclusions potentially inapplicable to patients who have not undergone preoperative treatment and were diagnosed via biopsy pathology. Future analyses should incorporate this specific patient population. Thirdly, the mutation of SMAD4 was assessed through immunohistochemical expression, which requires verification via polymerase chain reaction or genomic profiling to bolster detection accuracy. Lastly, there remains a lack of consensus regarding the cut-off values for CA19-9, leading to possible variations in research outcomes depending on the chosen threshold.

In conclusion, our study identifies SMAD4-mutated PDAC as a more aggressive subtype, characterized by a higher frequency of pathological fatty infiltration, peripheral nerve infiltration, and reduced recurrence-free survival. The presence of rim enhancement and CBD dilation on contrast-enhanced MRI, along with elevated CA19-9 levels, are significant imaging and clinical markers for distinguishing SMAD4-mutated PDAC. These findings contribute to the existing literature by offering insights into the radiological features associated with SMAD4 mutations, which could potentially reduce the need for invasive tissue sampling and aid in the development of personalized treatment strategies.

Abbreviations

PDAC	Pancreatic ductal adenocarcinoma.
DPC4	Deleted in pancreatic carcinoma.
TGF-β	Transforming growth factor-β.
BMI	Body mass index.
AJCC	The American Joint Committee on Cancer.
TBil	Total bilirubin.
RFS	Recurrence-free survival.
OS	Overall survival.
DWI	Diffusion-weighted images.
ADC	Apparent diffusion coefficient.
CBD	Common bile duct.
MPD	Main pancreatic duct.
IBD	Intrahepatic bile duct.

Supplementary Information

The online version contains supplementary material available at https://doi.org/10.1186/s12880-024-01539-3.

Supplementary Material 1

Acknowledgements

Not Applicable.

Author contributions

All authors contributed to the study conception and design. Material preparation, data collection and analysis were performed by Zhina Li, Cheng Wang, Xingxing Wang, Xiang Li, Tianzhu Yu, Jianjun Zhou, Xiaolin Wang, Mengsu Zeng, and Haitao Sun. The first draft of the manuscript was written by Zhina Li and Haitao Sun, and all authors commented on previous versions of the manuscript. All authors reviewed the manuscript.

Funding
This research was funded by "Science and Technology Innovation Action Plan" Star Cultivation (Sailing Program) (22YF1443600) and the China Postdoctoral Science Foundation (2023M732230).

Data availability
The datasets used and/or analyzed during the present study are available from the corresponding author on reasonable request.

Declarations

Ethical approval
This study was performed in accordance with the Declaration of Helsinki, and approved by the ethics committee of Zhongshan Hospital, Fudan university (B2024-250R), which waived the requirement for written informed consent owing to the use of deidentified retrospective data. Clinical trial number: not applicable.

Consent for publication
Not applicable.

Competing interests
The authors declare no competing interests.

Author details
[1]Department of Radiology, Zhongshan Hospital, Shanghai Institute of Medical Imaging, Fudan University, No. 180 Fenglin Road, Xuhui District, Shanghai 200032, China
[2]Department of Radiology, Linyi Centra Hospital, No.17 Jiankang Road, Linyi City, Shandong Province 276400, China
[3]Department of Pathology, Zhongshan Hospital, Fudan University, No. 180 Fenglin Road, Xuhui District, Shanghai 200032, China
[4]Department of Interventional Radiology, Zhongshan Hospital, No. 180 Fenglin Road, Xuhui District, Shanghai 200032, China
[5]Department of Radiology, Zhongshan Hospital (Xiamen), Xiamen Municipal Clinical Research Center for Medical Imaging, Fujian Province Key Clinical Specialty for Medical Imaging, Xiamen Key Laboratory of Clinical Transformation of Imaging Big Data and Artificial Intelligence, Fudan University, Xiamen 361015, China

Received: 4 October 2024 / Accepted: 17 December 2024
Published online: 23 December 2024

References

1. Halbrook CJ, Lyssiotis CA, Pasca Di Magliano M, Maitra A. Pancreatic cancer: advances and challenges. Cell. 2023;186(8):1729–54.
2. Grossberg AJ, Chu LC, Deig CR, Fishman EK, Hwang WL, Maitra A, Marks DL, Mehta A, Nabavizadeh N, Simeone DM, et al. Multidisciplinary standards of care and recent progress in pancreatic ductal adenocarcinoma. Cancer J Clin. 2020;70(5):375–403.
3. Yamazaki H, Streicher SA, Wu L, Fukuhara S, Wagner R, Heni M, Grossman SR, Lenz H, Setiawan VW, Le Marchand L, et al. Evidence for a causal link between intra-pancreatic fat deposition and pancreatic cancer: a prospective cohort and mendelian randomization study. CELL REP MED. 2024;5(2):101391.
4. Huang B, Huang H, Zhang S, Zhang D, Shi Q, Liu J, Guo J. Artificial intelligence in pancreatic cancer. THERANOSTICS. 2022;12(16):6931–54.
5. Dardare J, Witz A, Merlin JL, Gilson P, Harlé A. SMAD4 and the TGFβ pathway in patients with pancreatic ductal adenocarcinoma. INT J MOL SCI 2020, 21(10).
6. Zhao M, Mishra L, Deng CX. The role of TGF-β/SMAD4 signaling in cancer. INT J BIOL SCI. 2018;14(2):111–23.
7. Zhang J, Zuo CJ, Jia NY, Wang JH, Hu SP, Yu ZF, Zheng Y, Zhang AY, Feng XY. Cross-modality PET/CT and contrast-enhanced CT imaging for pancreatic cancer. WORLD J GASTROENTERO. 2015;21(10):2988–96.
8. Tascilar M, Skinner HG, Rosty C, Sohn T, Wilentz RE, Offerhaus GJ, Adsay V, Abrams RA, Cameron JL, Kern SE, et al. The SMAD4 protein and prognosis of pancreatic ductal adenocarcinoma. CLIN CANCER RES. 2001;7(12):4115–21.
9. Liang C, Shi S, Qin Y, Meng Q, Hua J, Hu Q, Ji S, Zhang B, Xu J, Yu X. Localisation of PGK1 determines metabolic phenotype to balance metastasis and proliferation in patients with SMAD4-negative pancreatic cancer. Gut. 2020;69(5):888–900.
10. Kassardjian A, Wang HL. SMAD4-Expressing Pancreatic Ductal Adenocarcinomas Have Better Response to Neoadjuvant Therapy and Significantly Lower Lymph Node Metastasis Rates. *PANCREAS* 2020, 49(9):1153–1160.
11. Principe DR, Underwood PW, Kumar S, Timbers KE, Koch RM, Trevino JG, Munshi HG, Rana A. Loss of SMAD4 is Associated with Poor Tumor Immunogenicity and reduced PD-L1 expression in pancreatic Cancer. FRONT ONCOL 2022, 12.
12. Wang Y, Yu T, Zhao Z, Li X, Song Y, He Y, Zhou Y, Li P, An L, Wang F. SMAD4 limits PARP1 dependent DNA repair to render pancreatic Cancer cells sensitive to Radiotherapy. CELL DEATH DIS. 2024;15(11):818.
13. Yao H, Luo L, Li R, Zhao Y, Zhang L, Pešić M, Cai L, Li L. New insight into the role of SMAD4 mutation/deficiency in the prognosis and therapeutic resistance of pancreatic ductal adenocarcinomas. Biochim et Biophys Acta (BBA) - Reviews Cancer. 2024;1879(6):189220.
14. Ronot M, Chernyak V, Burgoyne A, Chang J, Jiang H, Bashir M, Fowler KJ. Imaging to Predict Prognosis in Hepatocellular Carcinoma: Current and Future Perspectives. *RADIOLOGY* 2023, 307(3):e221429.
15. Jansen RW, de Bloeme CM, Cardoen L, Göricke S, van Elst S, Jessen JL, Ramasubramanian A, Skalet AH, Miller AK, Maeder P et al. MRI features for identifying MYCN -amplified RB1 wild-type Retinoblastoma. Radiology 2023:222264.
16. Kitao A, Matsui O, Zhang Y, Ogi T, Nakada S, Sato Y, Harada K, Yoneda N, Kozaka K, Inoue D, et al. Dynamic CT and Gadoxetic Acid-enhanced MRI characteristics of P53-mutated Hepatocellular Carcinoma. Radiology. 2023;306(2):e220531.
17. Patel SH, Batchala PP, Mrachek E, Lopes MS, Schiff D, Fadul CE, Patrie JT, Jain R, Druzgal TJ, Williams ES. MRI and CT Identify Isocitrate Dehydrogenase (IDH)-Mutant Lower-Grade Gliomas Misclassified to 1p/19q Codeletion Status with Fluorescence in Situ Hybridization. *RADIOLOGY* 2020, 294(1):160–167.
18. Bengtsson A, Andersson R, Ansari D. Histological variants of pancreatic ductal adenocarcinoma: a survival analysis. Langenbeck's Archives Surg 2024, 409(1).
19. Schawkat K, Tsai LL, Jaramillo-Cardoso A, Paez SN, Moser JA, Decicco C, Singer T, Glickman J, Brook A, Manning MA, et al. Use of ring-enhancement and focal necrosis to differentiate pancreatic adenosquamous carcinoma from pancreatic ductal adenocarcinoma on CT and MRI. CLIN IMAG. 2021;73:134–8.
20. Toshima F, Inoue D, Yoshida K, Yoneda N, Minami T, Kobayashi S, Ikdeda H, Matsui O, Gabata T. Adenosquamous carcinoma of pancreas: CT and MR imaging features in eight patients, with pathologic correlations and comparison with adenocarcinoma of pancreas. ABDOM RADIOL. 2016;41(3):508–20.
21. Attiyeh MA, Chakraborty J, McIntyre CA, Kappagantula R, Chou Y, Askan G, Seier K, Gonen M, Basturk O, Balachandran VP, et al. CT radiomics associations with genotype and stromal content in pancreatic ductal adenocarcinoma. ABDOM RADIOL. 2019;44(9):3148–57.
22. Hinzpeter R, Kulanthaivelu R, Kohan A, Avery L, Pham N, Ortega C, Metser U, Haider M, Veit-Haibach P. CT Radiomics and whole genome sequencing in patients with pancreatic ductal adenocarcinoma: predictive radiogenomics modeling. CANCERS. 2022;14(24):6224.
23. Bai X, Wu L, Dai J, Wang K, Shi H, Lu Z, Ji G, Yu J, Xu Q. Rim Enhancement and Peripancreatic Fat Stranding in Preoperative MDCT as predictors for Occult Metastasis in PDAC patients. ACAD RADIOL. 2023;30(12):2954–61.
24. Yoon SH, Lee JM, Cho JY, Lee KB, Kim JE, Moon SK, Kim SJ, Baek JH, Kim SH, Kim SH et al. Small (≤ 20 mm) pancreatic adenocarcinomas: analysis of enhancement patterns and secondary signs with multiphasic multidetector CT. *RADIOLOGY* 2011, 259(2):442–452.
25. Venkatesh SK, Welle CL, Miller FH, Jhaveri K, Ringe KI, Eaton JE, Bungay H, Arrivé L, Ba-Ssalamah A, Grigoriadis A, et al. Reporting standards for primary sclerosing cholangitis using MRI and MR Cholangiopancreatography: guidelines from MR Working Group of the International Primary Sclerosing Cholangitis Study Group. EUR RADIOL. 2022;32(2):923–37.
26. Lee S, Kim SH, Park HK, Jang KT, Hwang JA, Kim S. Pancreatic Ductal Adenocarcinoma: Rim Enhancement at MR Imaging Predicts Prognosis after Curative Resection. *RADIOLOGY* 2018, 288(2):456–466.
27. Sun H, Zhang S, Liu K, Zhou J, Wang X, Shen T, Song X, Guo Y, Wang X. MRI-based nomogram estimates the risk of recurrence of primary nonmetastatic pancreatic neuroendocrine tumors after curative resection. J MAGN RESON IMAGING. 2019;50(2):397–409.
28. Choi MH, Yoon SB, Lee YJ, Jung ES, Pak S, Han D, Nickel D. Rim enhancement of pancreatic ductal adenocarcinoma: investigating the relationship with DCE-MRI-based radiomics and next-generation sequencing. FRONT ONCOL. 2024;14:1304187.

29. Gao J, Chen X, Li X, Miao F, Fang W, Li B, Qian X, Lin X. Differentiating TP53 mutation status in pancreatic ductal adenocarcinoma using Multiparametric MRI-Derived Radiomics. FRONT ONCOL. 2021;11:632130.
30. Li Y, Basti A, Yalçin M, Relógio A. Circadian dysregulation of the TGFβ/SMAD4 pathway modulates metastatic properties and Cell Fate decisions in pancreatic Cancer cells. ISCIENCE. 2020;23(10):101551.
31. Hayashi A, Hong J, Iacobuzio-Donahue CA. The pancreatic cancer genome revisited. NAT REV GASTRO HEPAT. 2021;18(7):469–81.
32. Sinha R, Gardner T, Padala K, Greenaway JR, Joy D. Double-Duct sign in the clinical context. Pancreas. 2015;44(6):967–70.
33. Menges M, Lerch MM, Zeitz M. The double duct sign in patients with malignant and benign pancreatic lesions. GASTROINTEST ENDOSC. 2000;52(1):74–7.
34. Yadav P, Lal H. Double duct sign. ABDOM RADIOL. 2017;42(4):1283–4.
35. Takano S, Fukasawa M, Maekawa S, Kadokura M, Miura M, Shindo H, Takahashi E, Sato T, Enomoto N. Deep sequencing of cancer-related genes revealed GNAS mutations to be associated with intraductal papillary mucinous neoplasms and its main pancreatic duct dilation. PLoS ONE. 2014;9(6):e98718.
36. Han S, Kim JH, Yoo J, Jang S. Prediction of recurrence after surgery based on preoperative MRI features in patients with pancreatic neuroendocrine tumors. EUR RADIOL. 2022;32(4):2506–17.
37. Luo G, Jin K, Deng S, Cheng H, Fan Z, Gong Y, Qian Y, Huang Q, Ni Q, Liu C, et al. Roles of CA19-9 in pancreatic cancer: Biomarker, predictor and promoter. BBA-REV CANCER. 2021;1875(2):188409.
38. Yang J, Xu R, Wang C, Qiu J, Ren B, You L. Early screening and diagnosis strategies of pancreatic cancer: a comprehensive review. CANCER COMMUN. 2021;41(12):1257–74.
39. Kamisawa T, Wood LD, Itoi T, Takaori K. Pancreatic cancer. Lancet. 2016;388(10039):73–85.
40. Watanabe F, Suzuki K, Tamaki S, Abe I, Endo Y, Takayama Y, Ishikawa H, Kakizawa N, Saito M, Futsuhara K, et al. Longitudinal monitoring of KRAS-mutated circulating tumor DNA enables the prediction of prognosis and therapeutic responses in patients with pancreatic cancer. PLoS ONE. 2019;14(12):e0227366.

Publisher's note